SCIENTIFIC DATA

OPEN

Data Descriptor: Leukocyte Tracking Database, a collection of immune cell tracks from intravital 2-photon microscopy videos

Received: 24 July 2017
Accepted: 16 April 2018
Published: 17 July 2018

Diego Ulisse Pizzagalli[1,2], Yagmur Farsakoglu[1], Miguel Palomino-Segura[1], Elisa Palladino[1], Jordi Sintes[3], Francesco Marangoni[4], Thorsten R. Mempel[4], Wan Hon Koh[5], Thomas T. Murooka[5], Flavian Thelen[6], Jens V. Stein[6], Giuseppe Pozzi[7], Marcus Thelen[1], Rolf Krause[2] & Santiago Fernandez Gonzalez[1]

Recent advances in intravital video microscopy have allowed the visualization of leukocyte behavior *in vivo*, revealing unprecedented spatiotemporal dynamics of immune cell interaction. However, state-of-the-art software and methods for automatically measuring cell migration exhibit limitations in tracking the position of leukocytes over time. Challenges arise both from the complex migration patterns of these cells and from the experimental artifacts introduced during image acquisition. Additionally, the development of novel tracking tools is hampered by the lack of a sound ground truth for algorithm validation and benchmarking. Therefore, the objective of this work was to create a database, namely LTDB, with a significant number of manually tracked leukocytes. Broad experimental conditions, sites of imaging, types of immune cells and challenging case studies were included to foster the development of robust computer vision techniques for imaging-based immunological research. Lastly, LTDB represents a step towards the unravelling of biological mechanisms by video data mining in systems biology.

Design Type(s)	parallel group design
Measurement Type(s)	leukocyte migration trait
Technology Type(s)	digital imaging
Factor Type(s)	leukocyte • animal model of vaccine research • Imaging Region of Interest • Mouse Strains
Sample Characteristic(s)	Mus musculus • leukocyte

[1]Institute for Research in Biomedicine (IRB), Università della Svizzera italiana. Via Vincenzo Vela 6, 6500 Bellinzona, Switzerland. [2]Institute of Computational Science (ICS), Università della Svizzera italiana. Via Giuseppe Buffi 13, 6900 Lugano, Switzerland. [3]IMIM Hospital del Mar Medical Research Institute. Dr. Aiguader, 88, 08003 Barcelona, Spain. [4]Center for Immunology and Inflammatory Diseases, Massachusetts General Hospital. CNY 149-8 149 13th Street Charlestown, MA 02129, USA. [5]Department of Immunology, University of Manitoba. 471 Apotex Centre 750 McDermot Avenue, Winnipeg, MB R3E 0T5, Canada. [6]Theodor Kocher Institute (TKI), University of Bern. Freiestrasse 1, 3012 Bern, Switzerland. [7]Dipartimento di Elettronica, Informazione e Bioingegneria, Politecnico di Milano. P.za L da Vinci 32, I-20133 Milano, Italy. Correspondence and requests for materials should be addressed to R.K. (email: rolf.krause@usi.ch) or to S.F.G. (email: santiago.gonzalez@irb.usi.ch).

Background & Summary

Multi-Photon Intravital Video Microscopy (MP-IVM), in combination with image-based systems biology[1], represent a key methodology for studying the interplay of cells in organs and tissues of living animals[2]. Indeed, recent analyses of leukocyte migration in MP-IVM data, highlighted unprecedented cell-to-cell interaction patterns such as antigen capturing[3] and presentation[4], host-pathogen interaction[5,6], tumor immune surveillance[7] and cell activation[8] amongst others. The advantage of MP-IVM with respect to other optical methods relies on the usage of multiple infrared photons. The low energy of the photons allows a deep and point-wise excitation of the sample which reduces light scattering and limits photo-damage. These properties make MP-IVM suitable to capture 4D data with remarkable resolution, depth and prolonged periods of observation[9]. The most common image acquisition and analysis pipeline of MP-IVM data is depicted in (Fig. 1). Initially, an animal having fluorescent cells, is anaesthetized, and prepared for imaging by immobilization and surgical exposition of the organ of interest (Fig. 1a left). Then, 4D data, composed of parallel image planes at different depths, are acquired for several time instants (Fig. 1a right). After acquisition, data are analysed by detecting cells (Fig. 1b left), tracking their position over time (Fig. 1b right) and finally quantifying cell migration[10]. The described pipeline was used to generate all the entries proposed in the current work (Fig. 1d).

Despite the existence of specialized imaging software packages such as Imaris (Bitplane), Volocity (PerkinElmer) and FIJI[11], the automatic analysis of immune cell migration[10] in MP-IVM data is problematic. Challenges are introduced at each stage of the previously described pipeline and arise both from the complex biomechanical properties of leukocytes and from technical artifacts of *in vivo* imaging (Fig. 1,Table 1 and Fig. 2a). More specifically, high plasticity of cell shape, sustained speed and frequent contacts, set a limit on the capacity of detecting and tracking cells for long time periods[12]. Additionally, technical artifacts such as the variation and non-uniform diffraction of the light emitted by fluorescently-tagged cells or the physiological movement of the sample due to peristalsis, breathing or pulsing of blood vessels, further challenge the automatic analysis. Therefore, additional steps such as image pre-processing, tuning of software parameters and manual curation of tracks, are required to improve tracking results. As a consequence, usability of imaging software is reduced[13], bias introduced and the reproducibility of the results is compromised. An example is provided in (Fig. 2b) where the Track Speed Mean, Directionality,

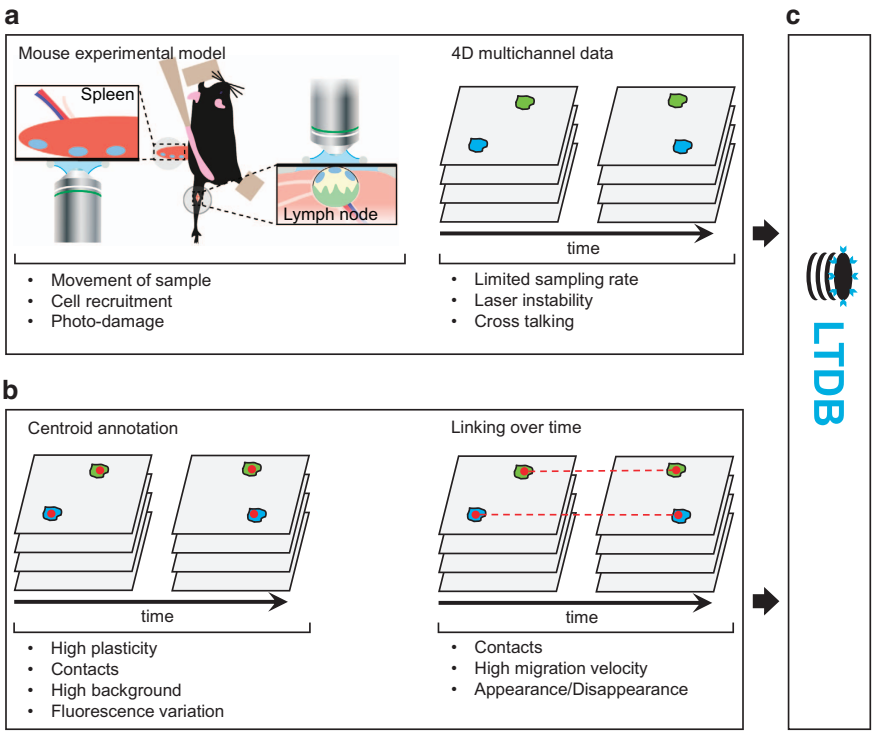

Figure 1. Data generation workflow. (**a**) *in vivo* imaging acquisition (left) Surgically exposed tissues from an anaesthetized and immobilized mouse are subjected to MP-IVM. (right) 4D data composed by z-stack of parallel image planes are acquired at different time points for multiple channels. (**b**) Cell detection and tracking (left) Cells are detected and the centroid position annotated the image series (red dots). Subsequently, (right) centroids are associated over time producing the cell tracks. For each phase of the imaging pipeline are reported specific problematics that affect cell tracking. **c**. Database. Both 4D imaging data and cell tracks are included in LTDB.

Problem	Description	Effect on cell detection and tracking
Plasticity (Pla)	High variability in cell shape, such as elongation and formation of protrusions	Parts of the same cell not detected or associated to other cells
Contact (Con)	Close proximity of two cells with the same color	Cells merged in a single object. Track interrupted or switched
High background or low signal to noise ratio (BG)	Background or other objects (collagen fibers, auto-fluorescence, cell debris) appear in the same channel of cells with a similar brightness	Inaccurate cell detection, track interruption, tracking of third objects
Fluorescence variation (Flu)	The intensity of fluorescent cells changes during acquisition. Reasons include photo-bleaching and migration in different areas of the tissue	Inaccurate cell detection and track interruption
High migrating velocity (Vel)	Migration velocity greater than the cell size in a time step (absence of overlap)	Track interruption and aliasing if assumptions for interpolation rules for poorly visible cells are not correct. Deformation of cell shapes
Appearance and Disappearance (A/D)	Sudden or progressive appearance/disappearance of a cell, either close to the boundaries of the field of view or in proximity to a blood or lymphatic vessel	Track duration is less or equal than the length of the video. Tracking errors if interpolation rules for poorly visible cells are not correct
Movement of the sample (Mov)	Shifting, drifting or fluctations of the sample due to the movement of the animal or insufficient isolation from breathing, peristalsis and heartbeat	Non-rigid deformation of the tissue, discontinuities in tracks
Microscope instability (Ins)	Noise introduced either by oscillations in the laser power or in the sensitivity of the photo-detectors, resulting in bands or bright spots	Detection of larger or smaller objects. Appearance of the background, disappearance of cells
Large areas (Lar)	Non-uniform brightness	Frequent detection and tracking errors if parameters are not adjusted locally. Increased computational time
Channel specificity (Spe)	Emitted spectrum is captured in more than one channel	Mis-detection and increased contacts with the background
Density (Den)	High number of cells in close proximity	Track switching for tightly interacting cells and mis-detection

Table 1. Biomechanical and technical problems. Description of the main problems for automatic cell detection and tracking. In brackets it is reported the abbreviation used to refer at each specific problem.

Track length and Track duration were computed for the entry LTDB017a (Data Citation 1). These values exhibited highly significant differences ($p \leq 0.0001$) between automatically-generated vs. manually-generated tracks.

Providing the scientific community with datasets interpreted by experts is essential to foster the development of data science methods. To this end, international cell tracking challenges on public datasets[14,15] allowed to highlight the properties amongst different algorithms. However, the provided datasets did not include leukocytes observed by intravital imaging. For this reason, it is necessary to develop an extended dataset of MP-IVM videos, where a significant number of leukocytes are tracked. Here we present a leukocyte tracking database, namely "LTDB", that includes MP-IVM videos of immune cells, together with their relative tracks which were manually annotated by experts. Each video contains one or more challenges for the automatic analysis (Table 2 (available online only)), and captured the behaviour of one or more cell populations (Table 3) in response to different stimuli (Table 4).

All the videos and tracks are made available as individual files or as a spatio-temporal database (Fig. 3a) which was optimized for faster access to data and metadata (Fig. 3b).

The expected usage of LTDB is to serve as a ground truth for the validation of tracking algorithms (Fig. 4a). Differences with respect to the ground truth can be evaluated using, for instance, a metric that accounts for complete tracking graph comparison[16].

LTDB further aims at being a training dataset for supervised machine learning methods. Indeed, in light of the recent application of deep learning for object detection and tracking in highly variable scenarios[17–19], LTDB can provide the large number of images-tracks pairs required for the training of predictive models (Fig. 4b). In this case, broad imaging conditions may support the generalization capabilities of these methods.

Although LTDB was provided to primarily enhance tracking algorithms, the database embeds biomedical knowledge. To this end, data-mining and image-based systems biology methods can be applied to correlate images, tracks and metadata for investigating properties of the immune system in health and disease (Fig. 4c).

Methods

Imaging data generation

Experiments were performed by four research groups using three customized two-photon microscopy platforms (Table 5). Either the splenic or the lymph-node surgical models were used for acquisition (Fig. 1a). Videos were acquired from 26 unique experiments, to observe the interplay of neutrophils, B cells, T cells and natural killer cells in innate or adaptive immune responses (Table 4).

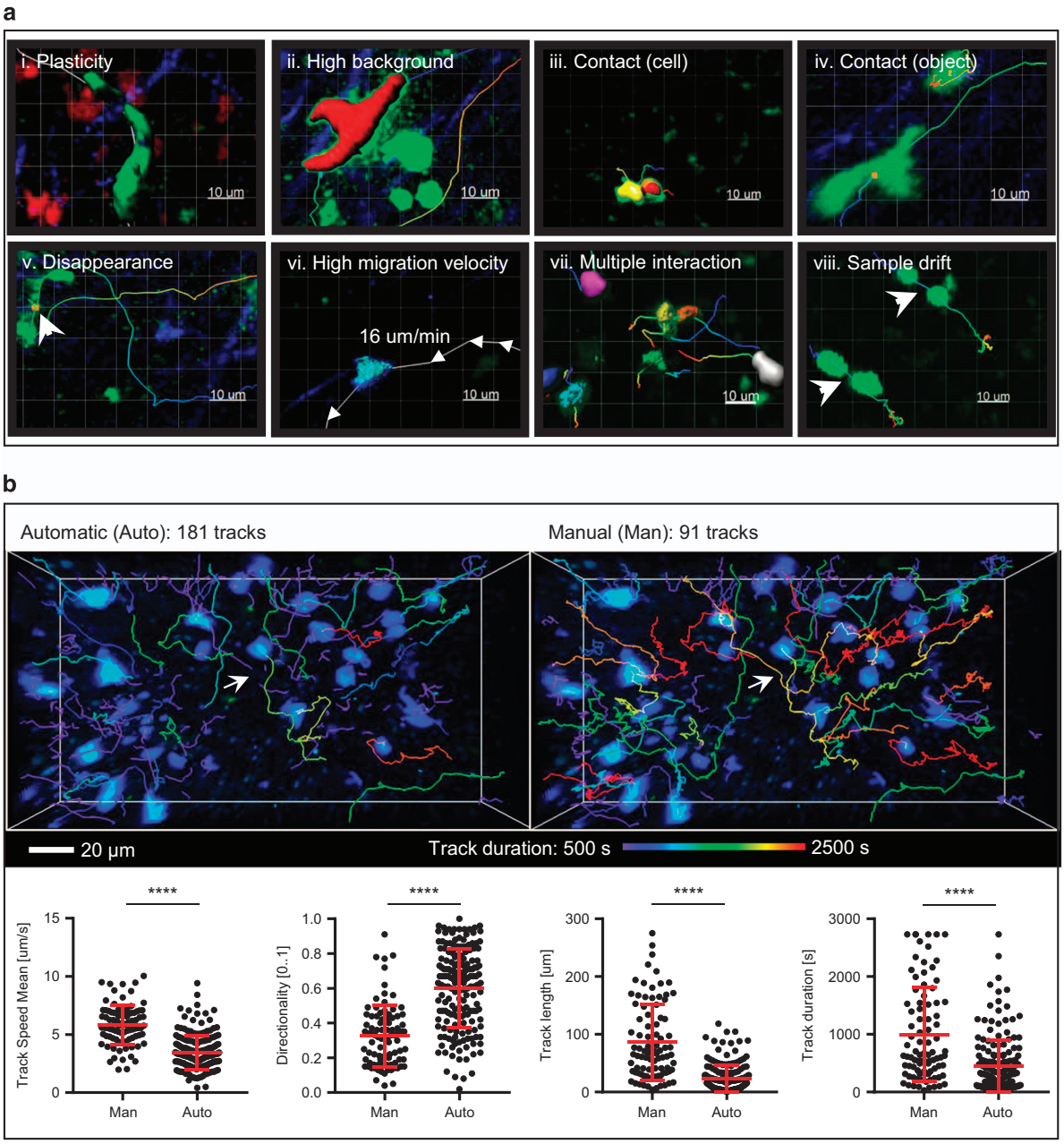

Figure 2. **Tracking challenges.** (**a**) Example case studies (i-viii) Representative snapshots of selected MP-IVM micrographs from problematic cases indicated in the upper part of the picture. (i) Surface reconstruction (SR) (green) of a T cell with uropodia. (ii) SR (red) of a T cell migrating with pseudopodia on a high background. (iii) SR (yellow, red) of two neutrophils forming a brief contact. (iv) Centers of mass (red dots) of a T cell forming a brief contact with a non motile object. (v) Estimated center of mass (red dot) of a T cell close to a boundary of the field of view. (vi) SR (blue) of a rapidly migrating Neutrophil. Arrows indicate cell displacement. (vii) SR (colored objects) of Neutrophils forming multiple contacts. (viii) Tracks (colored lines) of two B cells. (**b**) Effect of tracking errors Tracking errors limit research reproducibility, significantly ($p \leq 0.0001$) affecting the typical readouts from MP-IVM experiments. The figures (top-left and top-right) and the graphs (bottom) compare the manual tracks presented in *LTDB017_a* vs. the tracks generated automatically by Imaris. Automatic tracks were interrupted when the software could not detect or link cells, yielding to the creation of an increased number of shorter tracklets.

VideoID	CH0	CH1	CH2	CH3
CS001	BG(FR)	Tc(CMTMR)	**a:Tc(HIV-GFP)**	Coll
CS002	BG(FR)	Tc(CMTMR)	**a:Tc(HIV-GFP)**	Coll
CS003	BG(FR)	Tc(CMTMR)	**a:Tc(HIV-GFP)**	Coll
CS004	**a:Ne(UBC-CFP)**, Dc(CD11c YFP)	Vaccine	**a:Ne(UBC-CFP)**, Coll	
CS005	**a:Ne(UBC-GFP)**			
CS006	BG(FR)	Tc(CMTMR)	**a:Tc(HIV-GFP)**	Coll
CS007	**a:Ne(UBC-GFP)**			
CS008	**a:Ne(UBC-GFP)**			
CS009	**a:Ne(UBC-GFP)**			
CS010	**a:Ne(UBC-CFP)**, Dc(CD11c YFP)	Vaccine	**a:Ne(UBC-CFP)**, Coll	
CS011	**a:Ne(UBC-GFP)**, BG	BG	Coll, BG	
CS012	**a:Tc(CFSE)**			
CS013	**a:Ne(UBC-CFP)**, Dc(CD11c YFP)	Vaccine	**a:Ne(UBC-CFP)**, Coll	
CS014	**a:Ne(UBC-GFP)**	Vaccine	**a:Ne(UBC-CFP)**, Coll	
CS015	**a:Ne(UBC-CFP)**, Dc(CD11c YFP), AF	Ne(CMTMR), AF	**a:Ne(UBC-CFP)**, Coll, AF	
CS016	**a:Ne(UBC-CFP)**, Dc(CD11c YFP), AF	Ne(CMTMR), AF	**a:Ne(UBC-CFP)**, Coll, AF	
CS017	**a:Ne(UBC-CFP)**, Dc(CD11c YFP), AF	Ne(CMTMR), AF	**a:Ne(UBC-CFP)**, Coll, AF	
CS018	**a:NK(NCR1 GFP)**, Mp(CD169 Pe)	Mp(Cd169 Pe)	Vaccine	Coll
LTDB001	**a:Ne(UBC-CFP)**, Dc(CD11c YFP)	Vaccine	**a:Ne(UBC-CFP)**, Coll	
LTDB002	**a:Ne(UBC-CFP)**, Dc(CD11c YFP)	Vaccine	**a:Ne(UBC-CFP)**, Coll	
LTDB003	**a:Ne(UBC-CFP)**, Dc(CD11c YFP)	Vaccine	**a:Ne(UBC-CFP)**, Coll	
LTDB004	Ne(UBC-GFP), **a:Ne(UBC-CFP)**, AF	**b:Ne(CMTMR)**, AF	**a:Ne(UBC-CFP)**, Coll, AF	
LTDB005	Ne(UBC-GFP), **a:Ne(UBC-CFP)**, AF	**b:Ne(CMTMR)**, AF	**a:Ne(UBC-CFP)**, Coll, AF	
LTDB006	**a:Ne(UBC-CFP)**, Dc(CD11c YFP)	Vaccine, BG	**a:Ne(UBC-CFP)**, Coll	
LTDB007	**b:Ne(UBC-GFP)**, **a:Ne(UBC-CFP)**, AF	Ne(CMTMR), AF	**a:Ne(UBC-CFP)**, Coll, AF	
LTDB008	**a:Ne(UBC-CFP)**, Dc(CD11c YFP)	Vaccine	**a:Ne(UBC-CFP)**, Coll	
LTDB009	**a:Ne(UBC-CFP)**, Dc(CD11c YFP)	Vaccine	**a:Ne(UBC-CFP)**, Coll	
LTDB010	Ne(UBC-GFP), BG	**a:Bc(CTV)**		
LTDB011	**a:Ne(UBC-GFP)**, BG	Bc(CD19 RFP)		
LTDB012	BG(FR)	**a:Tc(CMTMR)**	**b:Tc(HIV-GFP)**	Coll
LTDB013	BG(FR)	Tc(CMTMR)	**a:Tc(HIV-GFP)**	Coll
LTDB014	**b:Bc(Bodipy 650)**	Tc(H2B-RFP)	Tc(NFAT-GFP)	**a:Bc(Ag+ Hoechst33342)**
LTDB015	Tc(CMAC)	**a:Tc(CFSE)**	Tc(CMTMR)	HEV(Meca-633)
LTDB016	**a:Ne(UBC-CFP)**, Dc(CD11c YFP)	Ne(CMTMR), AF	**a:Ne(UBC-CFP)**, Coll, AF	
LTDB017	**a:Ne(UBC-CFP)**, Dc(CD11c YFP)	Ne(CMTMR), AF	**a:Ne(UBC-CFP)**, Coll, AF	
LTDB018	Dc(CD11c YFP)	**a:NK(CMTMR)**		
LTDB019	**a:NK(CTV)**, Dc(CD11c YFP)	Vaccine	**a:NK(CTV)**	
LTDB020	BG	**a:NK(CMTMR)**	BG	Coll

Table 3. Channel specification Description of which cell population is expected to be visible in each channel of the provided videos. Bold indicates the cells that have been tracked. Brackets reports the type of staining used. The prefix a: or b: is used to indicate which is the corresponding tracking file (e.g. for video 04, b: N.(CMTMR) means that the tracks relative to the neutrophils labelled with CMTMR are in 04b.csv). Legend: Bc = B cells, Tc = T cells, Ne = neutrophils, Dc = dendritic cells, NKs = natural killer cells, Mp = macrophages, AF = auto-fluorescence, BG = background, Coll = collagen.

Data pre-processing

No image processing was applied to the provided videos. RAW images were also used for manual tracking. Cropping of large 4D volumes in space and/or time was performed for the entries of the case study collection to focus on the area of interest.

Manual tracking

Centroids of cells were manually annotated and linked over time, using the "Spots drawing" tool from Imaris (Bitplane). This process was performed by a group of three operators who tracked all the cells

VideoID	Site of Imaging	Immune stimulus	Group	Ref.
CS001	popliteal lymph node	HIV-infected humanized T cell	T.M. / T.T.M.	[5,25]
CS002	popliteal lymph node	HIV-infected humanized T cell	T.M. / T.T.M.	[5,25]
CS003	popliteal lymph node	HIV-infected humanized T cell	T.M. / T.T.M.	[5,25]
CS004	popliteal lymph node	Influenza Vaccine	S.F.G.	
CS005	spleen	Vaccinia Virus	S.F.G.	
CS006	popliteal lymph node	HIV-infected humanized T cell	T.M. / T.T.M.	[5,25]
CS007	spleen	Vaccinia Virus	S.F.G.	
CS008	spleen	Ovalbumin	S.F.G.	
CS009	spleen	Ovalbumin	S.F.G.	
CS010	popliteal lymph node	Influenza Vaccine	S.F.G.	
CS011	popliteal lymph node	Influenza Vaccine	S.F.G.	
CS012	popliteal lymph node	Steady State	J.V.S.	
CS013	popliteal lymph node	Influenza Vaccine	S.F.G.	
CS014	popliteal lymph node	Influenza Vaccine	S.F.G.	
CS015	popliteal lymph node	Influenza Vaccine	S.F.G.	
CS016	popliteal lymph node	Influenza Vaccine	S.F.G.	
CS017	popliteal lymph node	Influenza Vaccine	S.F.G.	
CS018	popliteal lymph node	Influenza Vaccine	S.F.G.	
LTDB001	popliteal lymph node	Influenza Vaccine	S.F.G.	
LTDB002	popliteal lymph node	Influenza Vaccine	S.F.G.	
LTDB003	popliteal lymph node	Influenza Vaccine	S.F.G.	
LTDB004	popliteal lymph node	Influenza Vaccine	S.F.G.	
LTDB005	popliteal lymph node	Influenza Vaccine	S.F.G.	
LTDB006	popliteal lymph node	Influenza Vaccine	S.F.G.	
LTDB007	popliteal lymph node	Influenza Vaccine	S.F.G.	
LTDB008	popliteal lymph node	Influenza Vaccine	S.F.G.	
LTDB009	popliteal lymph node	Influenza Vaccine	S.F.G.	
LTDB010	spleen	Ovalbumin	S.F.G.	
LTDB011	spleen	Ovalbumin	S.F.G.	
LTDB012	popliteal lymph node	HIV-infected humanized T cell	T.M. / T.T.M.	[5,25]
LTDB013	popliteal lymph node	HIV-infected humanized T cell	T.M. / T.T.M.	[5,25]
LTDB014	popliteal lymph node	Ovalbumin	T.M.	[7]
LTDB015	popliteal lymph node	Steady State	J.V.S.	
LTDB016	popliteal lymph node	Influenza Vaccine	S.F.G.	
LTDB017	popliteal lymph node	Influenza Vaccine	S.F.G.	
LTDB018	popliteal lymph node	Influenza Vaccine	S.F.G.	
LTDB019	popliteal lymph node	Influenza Vaccine	S.F.G.	
LTDB020	popliteal lymph node	Influenza Vaccine	S.F.G.	

Table 4. Experimental settings. Experimental conditions for each video. Ref. indicates the references for videos which are part of published works. The acronyms under the Group column correspond to S.F.G.: Santiago Fernandez Gonzalez group, T.M. / T.T.M.: Thorsten Mempel and Thomas T. Murooka group, J.V.S.: Jens V. Stein group

independently, redundantly and in three different locations without seeing the results produced by each other. In order to maximize track duration, cells were tracked also if partially visible. Tracks were interrupted only when cells completely disappeared. For specific studies, tracks of partially visible cells, migrating close to the boundaries of the field of view, can be excluded a posteriori by the user. Videos with ID (LTDB001 to LTDB020) have the maximum number of visible cells tracked. Videos in the Case Study collection (CS001 to CS018), instead, have only selected and challenging cells tracked.

Consensus tracking ground truth generation

Multiple independent annotations and tracks were merged into the consensus ground truth provided along with the dataset using a majority-voting scheme. This process was performed manually by a fourth expert using the "Unify" functionality of Imaris. The Matlab script LTDBCheck.m was used to facilitate

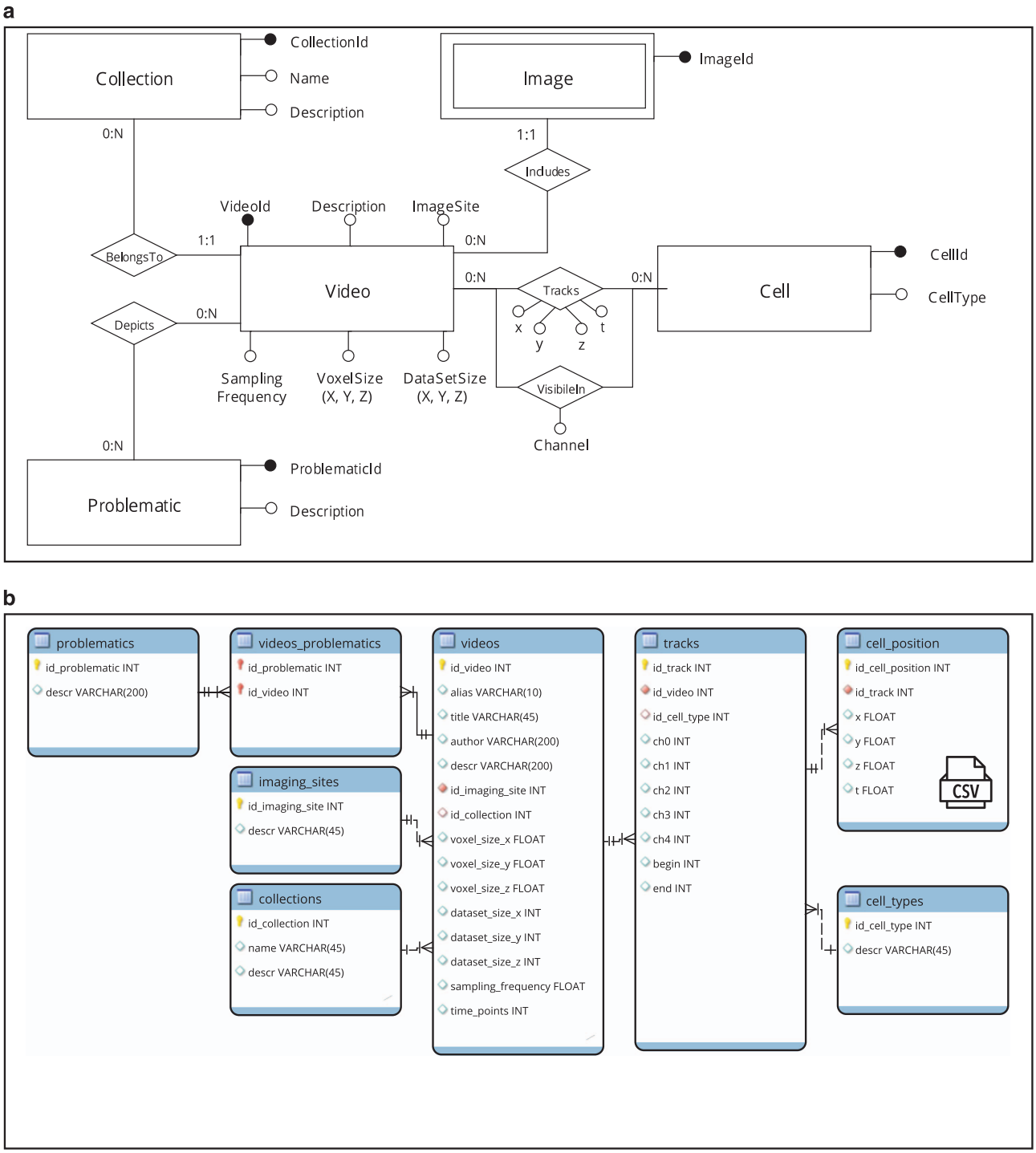

Figure 3. Data organization and formats. Videos, metadata and the position over time of tracked cells are organized as the conceptual Entity-Relationship model described in (**a**), corresponding to the logical database (optimized version) depicted in (**b**). A video belongs to a Collection, depicts one or more Problematic and includes an Image series. The Image entity is double-framed because it is a weak entity, which depends on the Video entity. A Cell has one type and one unique identifier. One Video tracks one (or more) Cell, every Cell being depicted by the Track association at a given timestamp (t) and in a spatial position (x, y, z) of that Video. The VisibleIn association further describes the channel of the video in which a cell is visible. The logical database is derived from the conceptual model and then optimized for read-access. The cells_positions table stores the instantaneous coordinates of each cell and is pre-exported in one or more CSV text files for each video. Imaging data are logically stored as TIFF image series with a specific filename.

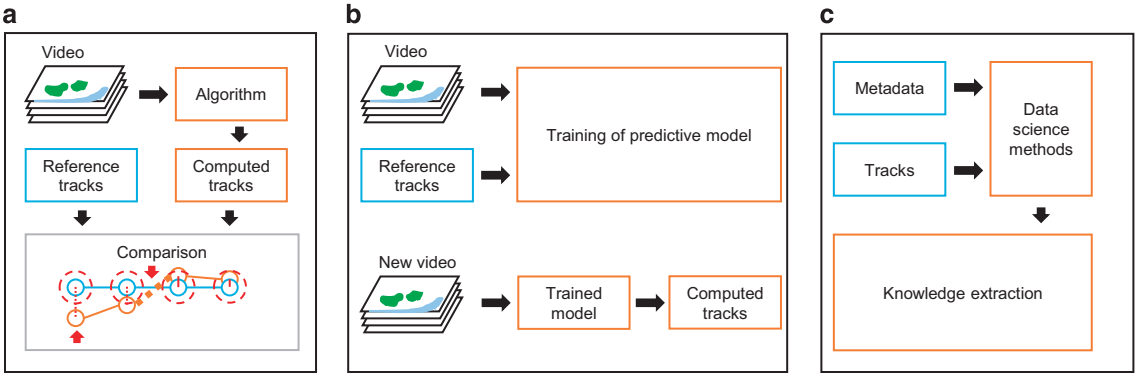

Figure 4. Typical usage scenarios. (**a**) Evaluation of a tracking algorithm. LTDB videos are provided as input to a tracking algorithm. Computed tracks can be compared with respect to the ground-truth tracks using a methodology of choice such as the complete graph comparison[15,16]. In the example red arrows indicate errors where a cell was detected not sufficiently close, and when a track was interrupted. (**b**) Machine learning dataset. LTDB videos and tracks can potentially be used in the context of supervised machine learning as training and validation dataset. The generated predictive model can be generalized and used to track new videos. (**c**) Resource for big data analysis. Properties of leukocyte migration in different experimental conditions can potentially be discovered by the application of pattern recognition on LTDB metadata and tracks.

track matching, detecting common errors and highlighting conflictive situations. Two tracks were said likely to "match" (i.e. referring to the same cell) if their annotations were closer than 10*um* for at least *N* time instants. *N* was defined as the minimum between the track duration and 10. Conflictive situations were detected as tracks matching for only certain time instants but not for the entire track duration. These include a) tracks with an annotation in a far position by mistake, b) a longer track matching with one or multiple shorter tracks, c) two tracks matching for *N* instants but having different initial and/or final positions (i.e. track switches for closely interacting cells) amongst others. Tracks with a duration shorter than 4 time instants were also inspected manually. Due to the high plasticity of cells these criteria were used only to facilitate the work of the fourth expert who had to manually merge multiple tracks as follows: If at least two operators agreed on the direction of a cell, the track was included in the dataset (i.e. two matching tracks having the same duration and detected in the same frames). If two operators tracked a cell, but the track duration was different, the points annotated only by one operator were evaluated, confirmed or discarded by the fourth expert. When two operators could not agree on the direction of a cell, the following method was applied. If the fourth expert or the Matlab script identified an evident tracking error (i.e. cells not annotated by mistake, unrealistic jumps or broken tracks) the error was corrected and the tracks were merged. For real conflictive situations (i.e. track switching for closely interacting cells) the experts were asked to meet and discuss the most appropriate solution. If still the majority consensus could not be reached, and only in this case, tracks were interrupted. Finally, the position of cell centroids included in the ground truth was not averaged but selected as the centroid closer to the mean. Although this choice may produce less smooth tracks, it avoids to position a centroid outside non-convex cells.

These criteria together with the manual merging of tracks and re-evaluation of tracking conflicts, allowed to include the maximum number of tracks for the longest possible period of time.

Animal models

The mouse strains included in this study are specified in Table 6 (available online only).

Prior to imaging, mice were anesthetized with a cocktail of Ketamine (100 mg/Kg) and Xylazine (10 mg/Kg) as previously described[4]. All animals were maintained in specific pathogen-free facilities at the Institute for Research in Biomedicine (Bellinzona, CH), Theodor Kocher Institute (Bern, CH) and Massachusetts General Hospital (Boston, MA). All the experiments were performed according with the rules and regulations of the local authorities and approved by the institutional animal committees: Swiss Federal Veterinary Office, Research Animal Care of the Massachusetts General Hospital, MGH Institutional Animal Care and Use Committee (IACUC).

Code availability

To facilitate the usage of LTDB, the following Matlab code is provided, under the GPL v3 Open Source licence, at http://www.ltdb.info/downloads/ or via Git-Hub at https://github.com/IRB-LTDB/.

`LTDBReadTracks.m` Reads the tracks contained in a CSV file.
`LTDBReadImages.m` Reads the 4D images contained in the TIFF files.
`LTDBExampleQuery.m` Provides an example for querying the locally installed database.

Microscope	Equipment	Format	VideoID
TrimScope (LaVision BioTec GmbH)	Ti:Sapphire lasers (Chamaleon Ultra I, Chamaleon Ultra II, CoherentInc.).Optical parametric oscillator (Chamaleon Compact OPO, Coherent Inc.), with 1010-1340nm emission and 690-1080nm output wavelength.	14 bits, 8 bits	CS004, CS005, CS007-CS011, CS013-CS018 LTDB001-LTDB011, LTDB016-LTDB020
Ultima IV multiphoton microscope (Bruker Systems)	DeepSee and MaiTai Ti:Sapphire lasers (Newport/Spectra-Physics) tuned between 850 and 990 nm.	12 bits	CS001-CS003, CS006; LTDB012-LTDB014
TrimScope (LaVision BioTec GmbH)	MaiTai Ti:Sapphire laser (Spectraphysics) tuned to 780 or 840 nm. Trimscope I based on BX50WI fluorescence microscope (LaVisionBiotec).	14 bits	CS012 LTDB015

Table 5. Microscopy platforms. Technical specifications of the MP-IVM microscopy platforms used to generate each video.

`XTLTDBImportTracks.m` Imports tracks as spots in Imaris.

`LTDB2C2C.m` Exports LTDB tracks in the format used for the Cell Tracking Challenge described in[14,15], mainly for evaluation with the methods proposed in[15].

`LTDBCheck.m` Checks for common tracking errors (i.e. annotations deleted by mistakes, broken tracks and overlapping tracks).

`EstimateDSMeasures.m` Estimates the measures in (Table 2 (available online only)) regarding the dataset complexity.

`LTDBCheck.m` and `EstimateDSMeasures.m` make use of the following libraries: ImarisReader (https://github.com/PeterBeemiller/ImarisReader) to read Imaris files and bwdistsc[20] to efficiently estimate the distance of each voxel from the closest centroid.

Data Records

Data included in this work (Videos and Tracks) are available through *figshare* (Data Citation 1)

Images resulting from MP-IVM are contained in two zip archives with name `TIFFS_LTDB001_LTDB020.zip` for the videos with ID 001 to 020, and in `TIFFS_CS001_CS018.zip` for the videos in the case study collection with ID 001 to 018. In these archives, a folder for each video contains 4D images as TIFF files.

Tracks resulting from the consensus tracking ground truth generation, are contained in the archive `GT_TRACKS.zip`

A dump of the SQL database used to organize data and metadata is provided in LTDB.sql.

The following supplementary files are available through *figshare* (Data Citation 1). For a quicker preview, each is available in a H264 encoded MP4 file named `<VideoID>.mp4`.

A snapshot of all the videos is contained in the archive SNAPSHOTS.zip respectively named `<VideoID>.png`

Individual tracks produced by different operators are provided in the supplementary archive `operator_individual_tracks.zip` and named `<VideoID>_<TrackID>_<OpID>.csv`. In this case `<OpID>` is the ID of the operator (OP1, OP2 or OP3).

Technical Validation

Imaging data

Imaging data were captured from organs of living animals using either the splenic or the popliteal lymph node surgical models (Fig. 1a and Table 4) which are typical for MP-IVM investigations of the immune system[2]. Cells involved in both innate and adaptive responses were included in the dataset. Videos 12, 13, 14 (Data Citation 1) come from recently published MP-IVM studies[5,7,21]. To represent data generated by multiple laboratories in different experimental settings[22], LTDB includes videos with different size, resolution, sampling rate and challenges for the automatic analysis (Table 2 (available online only)), acquired by three different microscopy platforms (Table 5). Moreover, cells were labelled with different fluorescent tags and detected by multiple channels (Table 3).

The following measures were computed to estimate the complexity of each video: signal to noise ratio (SNR), minimum distance between two cells (Dist) and number of cells per time instant. Since the proposed dataset is centroid-based rather than segmentation-based, SNR was estimated by adapting the definitions proposed in[15] with the following heuristic. Let $c_{i,t}$ be the centroid position of cell i at time t. For each voxel v in the current frame, the distance to the closest centroid was computed as $d_v = \min(||v - c_{i,t}||)\forall i$. Then, considering a typical cell diameter of $10um$, each voxel v was defined as foreground (FG-inside a cell) or background (BG-outside a cell) according with (Equation 1). This assumption allowed to sample a sufficient number of points in each video to estimate the aforementioned measures. (Table 2 (available online only)) summarizes the average values of each video while the

	TRA			Track duration				Number of tracks			
CS	**OP1**	**OP2**	**OP3**	**GT**	**OP1**	**OP2**	**OP3**	**GT**	**OP1**	**OP2**	**OP3**
001_a	1.00	0.87	0.86	30	30	30	30	1	1	1	1
002_a	0.90	0.98	1.00	119	119	79	119	1	1	2	1
003_a	0.99	0.99	1.00	118	117	118	118	1	1	1	1
004_a	1.00	1.00	1.00	18	18	18	18	1	1	1	1
005_a	0.99	1.00	1.00	22	22	22	22	2	2	2	2
006_a	1.00	0.96	0.95	119	119	118	119	2	2	2	2
007_a	0.61	1.00	0.69	26	27	26	28	13	7	13	8
008_a	1.00	0.99	0.99	111	111	90	91	2	2	3	3
009_a	1.00	1.00	1.00	114	114	114	114	4	4	4	4
010_a	1.00	0.99	0.99	25	25	22	22	3	3	4	4
011_a	0.84	1.00	0.75	37	44	37	35	6	4	6	5
012_a	0.85	1.00	0.93	15	16	14	16	9	7	10	8
013_a	1.00	1.00	0.98	38	38	38	38	1	1	1	1
014_a	0.38	0.95	0.96	185	179	88	203	4	1	9	5
015_a	1.00	0.97	0.98	184	184	179	180	1	1	1	1
016_a	0.97	0.97	1.00	155	153	157	155	1	1	1	1
017_a	1.00	1.00	1.00	116	116	116	116	2	2	2	2
018_a	1.00	0.59	0.48	42	40	52	42	15	16	7	7
LTDB	**OP1**	**OP2**	**OP3**	**GT**	**OP1**	**OP2**	**OP3**	**GT**	**OP1**	**OP2**	**OP3**
001_a	0.91	0.92	0.78	32	29	38	30	22	22	17	19
002_a	0.91	0.86	0.92	33	30	35	36	26	28	21	24
003_a	0.96	0.69	0.99	46	49	53	38	9	8	5	11
004_a	0.78	0.78	0.78	92	87	93	88	10	10	8	9
004_b	0.91	1.00	0.83	82	75	82	68	2	2	2	2
005_a	0.39	0.65	0.96	77	130	92	83	12	2	6	11
005_b	0.88	1.00	0.76	130	130	130	130	2	2	2	2
006_a	0.50	0.50	0.99	137	137	137	137	3	1	1	3
007_a	0.78	0.80	0.65	60	56	58	71	12	11	11	8
007_b	0.82	0.95	0.86	82	78	76	82	32	28	33	30
008_a	1.00	1.00	1.00	38	38	38	38	1	1	1	1
009_a	0.97	1.00	0.84	21	20	21	22	4	4	4	3
010_a	0.79	0.96	0.90	111	119	106	77	26	19	26	35
011_a	0.50	0.84	1.00	36	44	33	37	11	4	10	11
012_a	0.65	0.84	0.90	41	49	36	40	83	48	89	83
012_b	0.94	0.99	0.93	81	78	56	77	4	4	7	5
013_a	0.71	0.94	0.76	84	83	77	87	82	62	85	65
014_a	0.69	0.92	0.99	82	119	69	84	20	9	22	20
014_b	0.61	0.62	0.98	70	56	101	73	49	39	22	50
015_a	0.88	0.95	0.99	25	30	30	24	30	22	24	32
016_a	0.52	0.93	0.93	81	135	79	73	43	13	42	46
017_a	0.83	0.86	0.91	68	77	67	76	89	67	80	78
017_b	0.41	0.75	0.79	49	56	50	56	68	31	56	50
018_a	1.00	0.49	0.97	35	35	31	27	5	5	6	9
019_a	0.99	0.81	0.59	44	38	51	44	12	14	10	7
020_a	0.98	1.00	0.93	31	30	31	29	2	2	2	2
average	**0.84**	**0.89**	**0.90**	**71**	**74**	**68**	**70**	**17**	**12**	**15**	**15**

Table 7. Comparison of tracking operators Differences between the tracks produced by individual operators and the consensus ground truth, for all the videos in LTDB. Values of the TRA measure [15] close to 1 means the accurate matching of the operators tracks with respect to the consensus ground truth while lower values indicates tracking differences.

Row 1	VideoID [string]	dx [um]	dy [um]	dz [um]	dt [s]
	video identifier	*voxel size (x)*	*voxel size (y)*	*voxel size (z)*	*time interval*
Row 2	**ch0 [bool]**	**ch1 [bool]**	**ch2 [bool]**	**ch3 [bool]**	**ch4 [bool]**
	visible in channel 0	*visible in channel 1*	*visible in channel 2*	*visible in channel 3*	*visible in channel 4*
Rows 3 to end	**TrackID [string]**	**x [um]**	**y [um]**	**z [um]**	**t [INT]**
	unique track identifier	*position (x)*	*position (y)*	*position (z)*	*time instant*

Table 8. Structure of the CSV track file. The position of the centroids of all the cells tracked in a video was saved in a ASCII CSV file. Columns are delimited by the semicolon separator and rows are terminated by CR LF. The first row reports the identifier of the video, including the eventual suffix "a" or "b". The second to the fifth columns report the voxel size (dx,dy,dz) and the time interval (dt). The second row specifies in which channel (Ch) cells appear in the video. From the third to the last row, the coordinates of cells are saved. The first column represents the unique identifier of a track, not varying for the entire track duration. The second to fifth columns (x, y, z, t) represent the position of the cell with respect to the top-up-left most corner of the z-stack at a specific time point. Coordinates are expressed in μm while the time point is an integer number.

additional script `EstimateDSMeasures.m` can be used to compute the values for each time instant.

$$v \in FG \Rightarrow d_v < 4um \qquad v \in BG \Rightarrow d_v > 20um \tag{1}$$

$$SNR = \frac{||avg(FG) - avg(BG)||}{std(BG)} \tag{2}$$

Tracks

The consensus tracking ground truth provided with LTDB includes 728 unique tracks composed of 44722 instantaneous annotations. On average, each track is composed by 61 annotations. This varying with the track duration. The total observation time included in LTDB amounts to the equivalent of 260 hours for a single cell.

Common tracking errors (i.e. cells not annotated by mistake, broken tracks or jumps in the z-axis) as well as conflicts produced by multiple operators were detected by executing the Matlab script `LTDBCheck.m` provided in the code availability section.

Individual operators produced 1850 tracks (113807 annotations) which were merged into the 728 tracks of the consensus tracking ground truth. The performances of each operator with respect to the consensus ground truth is reported in (Table 7). To this end, the TRA[15] measure was computed. This measure includes a complete comparison of tracks represented as an acyclic oriented graph[16]. In order to estimate this measure, the ground truth and the individual tracks were converted in the format described in[15] and evaluated using the `TRAMeasure` software provided along. However, that software and methodology matches a cell in the ground-truth with a cell in the track to be evaluated, when they overlap more than 50% in space. Being our dataset centroid-based a difference of 1 voxel would made the matching not possible. Hence, considering the typical cell diameter, we approximated a sphere around each of the centroids. The tolerance radius of the spheres was at maximum of $10um$ and was truncated in case of two centroids closer than $10um$. The script `LTDB2CTC.m` was used to export the LTDB tracks in the acyclic oriented graph format described in[14,15].

Usage Notes

The expected use case scenario of LTDB is the evaluation of results produced by a cell tracking algorithm (Fig. 3a). Considering a generic cell tracking algorithm as an input-output system that reads an image sequence and outputs the tracks, LTDB can be used both as a source of images and as a ground truth for comparing the output.

To assess the overall performances of a cell tracking algorithm, we direct the user of LTDB towards the entries `LTDB001` to `LTDB020`. To test the behaviour of an algorithm on specific cases instead, we recommend the user with the videos in the Case Study collection `CS001` to `CS018` that facilitates manual investigation and debugging having a reduced number of cells.

4D images are provided as uint16 TIFF files. File names were structured as `<VideoID>_Txxx_Cxxx_Zxxx.tiff` where `<VideoID>` is either(LTDB001 to LTDB020 or CS001 to CS018), the suffix xxx after T, C, Z indicates time instant, channel number and depth level respectively and spans from 000 to 999 maximum. Images with a lower bit depth were stored as uint16 without any scaling. If needed, for normalization the bit-depth of each video can be found in (Table 2 (available online only)).

Tracks are provided in the CSV Format described in (Table 8) and named `<VideoID>_<TrackID>_GT.csv`. For videos with only one cell population `<TrackID>` is "a", while for videos

with two cell populations tracked it is either "a" or "b". These suffixes correspond to the suffixes used in (Table 2 (available online only)).

The synthetic example with `ID SQUARE` was added to the dataset. This provides a test-case for software having different coordinate systems. A parallelogram of $5 \times 5 \times 10um$ is positioned in the first frame close to the origin used for LTDB videos, corresponding to the bottom($x = 0$), left($y = 0$), deepest ($z = 0$) corner of the 3D volume. This parallelogram migrates along the y-axis.

In order to evaluate tracking performances we provide a Matlab script `LTDB2CTC.m` to export LTDB tracks as the acyclic oriented graph representation[16] used in the Cell Tracking Challenge described in[14,15]. This allows the usage of the accurate methodology and software provided by the aforementioned authors to compare computed tracks vs. ground truth.

For detecting cell populations visible in more than one channel (Table 2 (available online only) and Table 3) we encourage the usage of a co-localization method based on supervised machine learning such as Ilastik[23] or Trainable Weka Segmentation[24].

For discriminative machine learning models, it is worth noticing that all the cells of the videos `LTDB001` to `LTDB020` which are expected to be visible in the indicated channels were tracked. Other objects such as background, cell debris or additional cell populations were not tracked.

In the context of big-data analysis, (Fig. 3c) LTDB represents a resource to compare the biological properties of tracks (i.e. speed, directionality) amongst different experimental conditions. A review of the possible measures that could be computed from the tracks is provided in[10].

The SQL database `ltdb.sql` can be installed optionally and for instance using the MySQL database management system. Queries to retrieve videos of interest (i.e. associated to a specific challenge, type of cell or site of imaging) can be addressed to the locally installed database. Additionally, a web interface was set up to facilitate search, preview and download of videos and it is accessible at http://www.ltdb.info/

References

1. Medyukhina, A, Timme, S, Mokhtari, Z. & Figge, M. T. Image-based systems biology of infection. *Cytometry Part A* **87,** 462–470 (2015).
2. Stein, J. V. & Gonzalez, S. F. Dynamic intravital imaging of cell-cell interactions in the lymph node. *Journal of Allergy and Clinical Immunology* **139,** 12–20 (2017).
3. Gonzalez, S. F. *et al.* Capture of influenza by medullary dendritic cells via sign-r1 is essential for humoral immunity in draining lymph nodes. *Nature immunology* **11,** 427–434 (2010).
4. Mempel, T. R, Henrickson, S. E. & Von Andrian, U. H. T-cell priming by dendriticcells in lymph nodes occurs in three distinct phases. *Nature* **427,** 154–159 (2004).
5. Murooka, T. T. *et al.* Hiv-infected t cells are migratory vehicles for viral dissemination. *Nature* **490,** 283–287 (2012).
6. Chatziandreou, N. *et al.* Macrophage death following influenza vaccination initiates the inflammatory response that promotes dendritic cell function in the draining lymph node. *Cell Reports* **18,** 2427–2440 (2017).
7. Marangoni, F. *et al.* The transcription factor nfat exhibits signal memory during serial t cell interactions with antigen-presenting cells. *Immunity* **38,** 237–249 (2013).
8. Mandl, J. N, Torabi-Parizi, P. & Germain, R. N. Visualization and dynamic analysis of host-pathogen interactions. *Current opinion in immunology* **29,** 8–15 (2014).
9. Helmchen, F. & Denk, W. Deep tissue two-photon microscopy. *Nature methods* **2,** 932–940 (2005).
10. Beltman, J. B, Marée, A, F. & de Boer, R. J Analysing immune cell migration. *Nature Reviews Immunology* **9,** 789–798 (2009).
11. Schindelin, J. *et al.* Fiji: an open-source platform for biological-image analysis. *Nature methods* **9,** 676–682 (2012).
12. Zimmer, C. *et al.* On the digital trail of mobile cells. *IEEE Signal Processing Magazine* **23,** 54–62 (2006).
13. Carpenter, A. E, Kamentsky, L. & Eliceiri, K. W. A call for bioimaging software usability. *Nature methods* **9,** 666 (2012).
14. Maška, M. *et al.* A benchmark for comparison of cell tracking algorithms. *Bioinformatics* **30,** 1609–1617 (2014).
15. Ulman, V. *et al.* An objective comparison of cell-tracking algorithms. *Nature methods* **14,** 1141 (2017).
16. Matula, P. *et al.* Cell tracking accuracy measurement based on comparison of acyclic oriented graphs. *PloS one* **10,** e0144959 (2015).
17. Lempitsky, V. & Zisserman, A. Learning to count objects in images. In *Advances in Neural Information Processing Systems* 1324–1332 (2010).
18. Nam, H. & Han, B. Learning multi-domain convolutional neural networks for visual tracking. In *Proceedings of the IEEE Conference on Computer Vision and Pattern Recognition* 4293–4302 (2016).
19. Milan, A, Rezatofighi, S. H, Dick, A, Reid, I. & Schindler, K. Online multi-target tracking using recurrent neural networks. *arXiv preprint arXiv:1604.03635* (2016).
20. Mishchenko, Y. A function for fast computation of large discrete euclidean distance transforms in three or more dimensions in matlab. signal. *Image and Video Processing* **9,** 19 (2015).
21. Sharaf, R, Mempel, T. R. & Murooka, T. T. Visualizing the behavior of hiv-infected t cells in vivo using multiphoton intravital microscopy. *HIV Protocols* 189–201 (2016).
22. Meijering, E., Carpenter, A. E., Peng, H., Hamprecht, F. A. & Olivo-Marin, J.-C. Imagining the future of bioimage analysis. *Nature biotechnology* **34,** 1250 (2016).
23. Sommer, C, Straehle, C, Köthe, U. & Hamprecht, F. A.Ilastik: Interactive learning and segmentation toolkit *IEEE international symposium on biomedical imaging: From nano to macro* 230–233, (2011).
24. Arganda-Carreras, I. *et al.* Trainable weka segmentation: a machine learning tool for microscopy pixel classification. *Bioinformatics* **33,** 2424–2426 (2017).
25. Brainard, D. M. *et al.* Induction of robust cellular and humoral virus-specific adaptive immune responses in human immunodeficiency virus-infected humanized blt mice. *Journal of virology* **83,** 7305–7321 (2009).

Data Citation

1. Pizzagalli, D. U. *et al. Figshare* https://dx.doi.org/10.6084/m9.figshare.c.3827890 (2018).

Acknowledgements

We are thankful to Nikolaos Chatziandreou, Michael Bronstein and Davide Eynard, Benedikt Thelen, Sonia Pozzi for technical discussion and support, Rocco D′Antuono, Diego Morone and the IRB imaging facility for microscopy assistance, Tommaso Virgilio, Irene Latino, Ilaria Pierangeli, Ilaria Arini and Radu Theodorescu for help during manual tracking. This project was supported financially by Systemsx.ch the Swiss Initiative in Systems Biology with the grant 2013/124, by the Swiss National Foundation (SNF) with the grant Ambizione 148183 to S.F.G., by the Marie Curie Reintegration Grant 612742 to S.F.G. and partially by the Center for Computational Medicine in Cardiology (CCMC) at ICS.

Author Contributions

D.U.P. designed the database, analysed the data, developed the technical infrastructure and wrote the manuscript. M.P.-S., Y.F., E.P., J.S., F.T., J.V.S. F.M., T.M., W.H.K., T.T.M. conducted MP-IVM experiments, analysed the data and revised the manuscript. M.T. supported the development and discussion of the entire project. G.P. revised the structure of the database. R.K. supervised the technical aspects of the project. S.F.G. supervised the whole project and wrote the manuscript.

Additional Information

Tables 2 and 6 are available only in the online version of this paper.

Competing interests: The authors declare no competing interests.

How to cite this article: Pizzagalli, D. U. *et al.* Leukocyte Tracking Database, a collection of immune cell tracks from intravital 2-photon microscopy videos. *Sci. Data* 5:180129 doi: 10.1038/sdata.2018.129 (2018).

Publisher's note: Springer Nature remains neutral with regard to jurisdictional claims in published maps and institutional affiliations.